Talanta 296 (2026) 128482

Contents lists available at ScienceDirect

Talanta

journal homepage: www.elsevier.com/locate/talanta

Quantitative approaches for spatial metabolomics with isomer differentiation using surface sampling capillary electrophoresis mass spectrometry

Anastasia Golubova, Ingela Lanekoff *

Department of Chemistry – BMC, Uppsala University, 75 123, Uppsala, Sweden

ARTICLE INFO

Keywords:
Capillary electrophoresis-mass spectrometry
Spatial metabolomics
Quantitative metabolomics
Brain tissue section analysis

ABSTRACT

The importance of metabolites and their isomeric structures in biological function and dysfunction is increasingly recognized. However, achieving quantitative mapping of metabolites within tissue regions, particularly with isomeric specificity, remains an analytical challenge. This work presents the development of a quantitative surface sampling capillary electrophoresis method for spatial metabolomics with isomeric resolution. Five quantitation strategies were evaluated, with the optimal approach identified as sequential injection of metabolites directly from tissue alongside standards. This methodology was applied to a rat brain tissue section in a proof-of-principle study, enabling quantitative spatial analysis of metabolites, neurotransmitters, and isomeric species. Among the findings, the aromatic amino acids tyrosine, phenylalanine, and tryptophan exhibited the most dynamic distributions across four brain regions, while leucine and isoleucine demonstrated distinct spatial profiles, with leucine consistently being the more abundant isomer. This method offers a promising tool for advancing the understanding of spatially resolved biochemical processes underlying biological function and dysfunction.

1. Introduction

Spatial metabolomics enables mapping of analytes to specific localizations in thin tissue sections, thus providing an additional dimension to metabolomics performed as bulk analysis of homogenized tissue. Spatial molecular profiling can be achieved through mass spectrometry imaging (MSI) where analytes are mapped in pixels over the tissue [1,2]. In MSI, analytes are desorbed/sputtered/extracted directly from discrete locations over the tissue section for subsequent ionization and mass spectrometric detection. However, the metabolome of tissue is highly complex with isomeric and isobaric species, which may require sophisticated mass spectrometric methods to resolve [3–8]. Alternatively to MSI, spatial metabolomics of larger regions on tissue can be performed by physically removing tissue regions for analysis through dissection, including macrodissection, microdissection, or laser microdissection [9,10]. Following, the dissected tissue is prepared for following analysis using liquid chromatography (LC), gas chromatography (GC), or capillary electrophoresis (CE) coupled to mass spectrometry (MS). This approach offers an opportunity to obtain spatial information of molecules with high structural confidence.

The third alternative for spatial metabolomics is to use techniques that combine direct surfaces sampling of analytes from the tissue with separation prior to MS. These techniques are mainly based on desorbing analytes into a solvent for later analysis with LC-MS or CE-MS [11–16]. In addition to eliminating a laborious sample preparation, which is often required for dissected tissue, the direct surface sampling techniques enable in-depth chemical characterization of analytes from distinct cellular regions in tissue without additional steps. For example, analytes from a discrete location on mimetic tissue were sampled and analyzed with LC-MS to successfully separate and detect the isomers leucine and isoleucine [17]. Separation of isomers is important in metabolomics since they can have vastly different biological function: for instance, leucine helps to maintain muscles by stimulating protein production while isoleucine participates in hemoglobin synthesis [18]. The combination of high structural confidence with spatially resolved information thereby offers information on important functions of cellular regions in biological systems.

In addition to the ability to differentiate and detect isomers and

This article is part of a special issue entitled: Frontiers in electrophoresis published in Talanta.

* Corresponding author. Dept. of Chemistry-BMC, Uppsala University, 576, 751 23, Uppsala, Sweden.
E-mail address: Ingela.Lanekoff@kemi.uu.se (I. Lanekoff).

https://doi.org/10.1016/j.talanta.2025.128482
Received 27 September 2024; Received in revised form 9 June 2025; Accepted 16 June 2025
Available online 18 June 2025

isobars, a full interpretation of their biological significance requires knowledge of their quantity. Quantitation in direct infusion surface sampling techniques, such as MSI, is challenging because of the inherently altered chemical gradients and morphological structures in tissue that influence metabolite ionization [19,20]. The three main approaches for quantitation in MSI are: 1) spray an internal standard on top of the tissue [21], 2) include internal standards (IS) in the solvent for sampling with liquid extraction [22,23], or 3) make an external calibration curve using standards spiked in a mimetic tissue model [24]. As in all quantitative measures, it is essential to relate the signal of the analyte to a standard to learn the amount and not solely rely on detected ion intensities [25,26]. Furthermore, for spatial metabolomics techniques, including MSI, analytes are quantified after they have been desorbed into the extraction solvent or after they have been ablated from the surface. Thus, the amount in the tissue remains unknown since the yield of extraction or ablation from the tissue is not known.

Quantitation of analyte amounts in the tissue has been reported using the liquid microjunction surface sampling probe (LMJ SSP) coupled to LC-MS. In one study, the probe was parked at individual spots to exhaustively sample individual spots on the tissue for subsequent LC-MS. By doping the sampling solvent with internal standards, quantitation was performed in each spot with using one-point calibration [27]. In another study, the results from LMJ SSP LC-MS were compared with LC of tissue spots that had been physically punched out from the tissue section and into a vials for analyte extraction through sonication [14,28]. Thus, despite that none of these approaches for spatial metabolomics actually determine the extraction efficiency, the effect of analyte extraction from the tissue is taken into account.

We have previously reported surface sampling (SS) CE-MS for untargeted spatial metabolomics and separation of isomeric metabolites from tissue locations [13,16]. In SS-CE-MS the material is directly sampled from the tissue surface and consequently injected into the separation capillary. Here, we present and evaluate several strategies for acquiring quantitative data of detected analytes desorbed into the solution directly from tissue. These strategies including external calibration curves using mimetic tissue and internal standard methods. We discuss and experimentally evaluate these strategies and apply the optimal quantitative methodology using sequentially injected internal standards to profile and quantify endogenous metabolites and isomers desorbed from four morphological regions of rat brain tissue.

2. Materials and methods

2.1. Biological sample preparation

Rat brain (Rat Sprague Dawley Brain, obtained from Innovative Research, Novi, USA) was used in three different ways: 1) an extract was prepared by homogenizing 1.17607 g of tissue in 33.976 mL of methanol and collecting the supernatant after centrifugation. 2) A mimetic tissue was prepared, as described elsewhere [24]. Briefly, rat brain was cut, homogenized into a uniform mass with beads, and the homogenate was divided into 4 portions. Three portions were spiked with γ-aminobutyric acid-2,2-d2 (GABA-d2) (concentrations in Table S5), mixed, and layered in a plastic mold. The mimetic tissue was then frozen, cryosectioned, and thaw mounted on regular glass slides. 3) Rat brain tissue was cryosectioned into 12 μm thick sections and thaw mounted onto regular glass slides.

2.2. Chemicals

The background electrolyte (BGE) was prepared using HPLC-MS grade methanol (BDH Chromanorm Solvents), deionized water (18.2 MΩ, Milli-Q, Millipore), and formic acid (98–100 %, Merck, Germany). Standard solutions were prepared from γ-aminobutyric acid (GABA), GABA-2,2-d2, cell free amino acid mixture- 15 N, acetylcholine (N,N,N-trimethyl-d9) (all from Sigma-Aldrich), and L-carnitine-HCl (methyl-d3) (Larodan). Stock solution of GABA-d2 at 105.3 μM was prepared in BGE (MeOH:H2O 50:50, 1 % formic acid). For calibration curves in BGE and brain extract, 3 standard solutions containing GABA-d2 were prepared by mixing the GABA-d2 stock solution with BGE or brain extract (concentrations in Table S1 and S3, respectively). Solutions of isotopically labelled standards for one-point calibration were prepared in BGE at the concentrations 69.1 μM GABA-d2, 23.3 μM carnitine-d3, 11.3 μM acetylcholine-d9 and ^{15}N labelled amino acid mixture ranging from 5.4 μM (histidine) to 81.7 μM (alanine) (Table S9).

2.3. SS-CE-MS setup

The SS-CE-MS system was set up as previously described [13]. Briefly, a fused silica capillary (50 cm length, 150 μm OD and 50 μm ID, GENETEK, Sweden) was coupled to ESI-MS using a co-axial sheath flow liquid interface and positioned at an angle to a stainless steel capillary (7 cm length, 130 μm OD and 50 μm ID, MS Ekspert, Poland) over the sample surface. The sample was moved into position using computer controlled linear XYZ stages (Zaber Technologies Inc, Canada). The extraction droplet was formed manually by propelling a solvent through a plastic tube connected to stainless steel union (which holds BGE delivery capillary) with a syringe and syringe pump. The size and formation of the droplet was visually controlled with a digital camera (Dino-Lite, USA) and was deemed good when the droplet served as a bridge between the capillaries. Following, the probe was placed on the targeted region of the sample, which position was monitored vizually using a digital camera (Dino-Lite, USA), and analytes were electrokinetically injected in the CE separation capillary by applying 22 kV (Spellman SL10, New York, USA) for 15 s. After injection, the capillary assembly was moved to a vial with BGE and 22 kV was applied for CE separation prior to MS. For sampling and analysis of standards, 2 μL of standard solution was placed on a glass slide and electrokinetically injected into the separation capillary using the same probe and experimental setup as for direct tissue sampling.

2.4. Mass spectrometry and data analysis

A QExactive Orbitrap (ThermoFisher) was operated in full scan positive mode between 70 and 1000 Da at a resolution of 140 000 ($m/\Delta m$ at m/z 200) in all experiments. The electropherograms and mass spectra were analyzed in ThermoFisher Xcalibur QualBrowser and all peak areas were extracted manually. For extraction of migration times and intensities, Thermo RAW files were converted to centroid mzXML files using MSConvertGUI (ProteoWizard) and run through custom written Matlab scripts with a mass tolerance set to 5 ppm. Peak identification was performed either by (relative) migration time using standards or tentatively by accurate mass obtained from databases (HMDB, Metlin). Two-tailed Student's t-test was used for comparison of metabolite concentrations between brain regions.

3. Results and discussion

Spatial metabolomics using SS-CE-MS generates data of various metabolites, including isomeric and isobaric species [13,16]. To evaluate quantitative approaches with SS-CE-MS, selected isotopically labelled standards were used both for liquid and solid samples. In a first experiment, the quantitative response obtained with the SS-CE-MS set up was evaluated using an external calibration curve from liquid standard solutions of GABA-d2 and GABA. GABA-d2 was added at varying concentrations to a constant concentration of 70.1 μM GABA in each standard solution for the analysis in three technical replicates of each solution (Fig. S1, Table S1 and S2). The raw data for both GABA and GABA-d2, shows a relative standard deviation (RSD) of 30–40 % and a coefficient for determination (R2) value of 0.936 (Table S2, Fig. S1A). The high variation is often observed in electrokinetic injection without standard normalization due to injection bias as discussed in the

literature [29]. The analytes GABA and GABA-d2 have similar migration and the minimal RSD of <3 % that is achieved when GABA-d2 is normalized to GABA support that the main variability lay in the electrokinetic injection (Fig. S1B, Table S2). Thus, the SS-CE-MS system behaves similarly as a regular CE-MS system with electrokinetic injection and is equally capable of generating a linear external calibration curve with internal standards for quantitation.

In a second experiment, the chemical complexity was increased by adding GABA-d2 to a methanolic rat brain extract. To imitate the similar chemical matrix and environment as in tissue, the brain extract was diluted until the signal for endogenous GABA was close to the value obtained using SS-CE-MS for analysis of brain tissue sections [13]. Varying concentrations GABA-d2 were spiked into a constant amount of brain extract to keep the endogenous GABA ($GABA_{end}$) concentration constant (Table S3). The increased chemical complexity results in higher RSD's (21–107 %) while the RSD of GABA-d2/$GABA_{end}$ remains less than 3 % over the entire range (Fig. 1A, Table S4). This demonstrates that the electrokinetic injection is affected by increased chemical complexity in the solution and the matrix composition, although the GABA and GABA-d2 are affected to the same extent.

In a third experiment, the analytical complexity was increased by sampling from the surface of a mimetic tissue model. Mimetic tissue has been used for quantification methods in MSI [30] and is generated from homogenized tissue. The use of mimetic tissue model enables the entire process of SS-CE-MS analysis, from sampling to detection, to be evaluated since the process includes both desorption of analytes from the tissue into the micro-droplet and electrokinetic injection of the desorbed analytes into the capillary [13,16]. The tissue model contained four layers, where one layer was blank and the other three layers contained increasing concentrations of GABA-d2 (Table S5). The quantitative ability of SS-CE-MS from the sample surface was evaluated by sampling each layer three times using similarly sized droplets of 30–40 nL (Table S6 and S7, Fig. S2). The results show that the RSD for GABA-d2 and GABA is between 18 and 42 %, which is similar to data acquired from clean standard solutions and lower than data acquired from solutions with complex samples (Table S6). However, the RSD for the lowest concentration of GABA-d2 was almost 20 %, which is attributed to the low signals of GABA-d2 (Fig. 1B–Table S6). Although this shows the difficulty in using mimetic tissue models, the added complexity of extraction from the sample surface did not increase the variability.

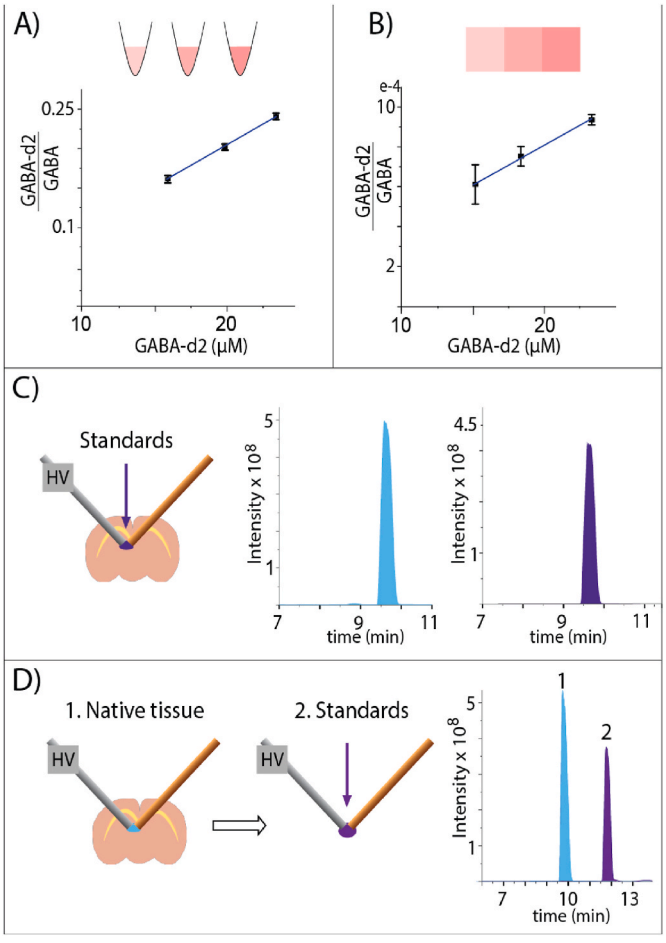

Fig. 1. Four different strategies for quantification using SS-CE-MS from chemically complex samples. a) External calibration curve for GABA-d2 spiked in brain extract; b) external calibration curve for GABA-d2 spiked in mimetic tissue; c) on-line simultaneous injection of GABA-d2 with tissue surface sampling; d) off-line sequential injection of GABA-d2 after tissue surface sampling and ~1,5 min of BGE. In c) and d) endogenous GABA (m/z 104. 0710) is depicted in blue and GABA-d2 (m/z 106.0835) in purple. Error bars in a) and b) correspond to one standard deviation (n = 3). (For interpretation of the references to colour in this figure legend, the reader is referred to the Web version of this article.)

In a fourth experiment, a regular thin rat brain tissue section was used for SS-CE-MS. In this approach, GABA-d2 was added into the extraction solvent, similar to quantitation performed with MSI and spatial metabolomics [23,27]. Specifically, GABA-d2 was added to the extraction solvent at a known concentration prior to sampling and was therefore sampled and analyzed together with the analytes from the tissue surface (Fig. 1C). Thus, the electropherogram contained both the endogenous GABA and the GABA-d2 as illustrated by blue and purple traces, respectively (Fig. 1C). Following, quantitation of $GABA_{end}$ was achieved using a one-point calibration where the peak area ratio of $GABA_{end}$ to GABA-d2 was multiplied with the concentration of GABA-d2 (Fig. 1C–Table S8). However, the suitability of this approach was limited by needing to add GABA-d2 into the extraction solvent. Furthermore, direct contact of internal standards with the tissue was found to contaminate the system, which limited the performance of unbiased independent replicates. Nevertheless, this on-line approach was found to be much simpler and less time and sample consuming compared to generating a mimetic tissue model.

In a fifth experiment, GABA-d2 was instead loaded after the extraction of endogenous analytes with a BGE gap between the injections, which is referred to as multisegmented electrokinetic injection. We have previously reported using multisegmented electrokinetic injection for SS-CE-MS [13], and others have reported robust multisegmented hydrodynamic injection of standards in liquid to build external calibration curves and quantify metabolites in serum [31]. In this workflow, a regular rat brain tissue was first sampled with SS-CE-MS. Following, the probe was placed in BGE to create a 1–1.5 min gap, and subsequently a standard solution containing GABA-d2 was sampled. Once both the tissue and the standard solution were sampled, the separation occurred simultaneously with a time gap in the separation capillary (Fig. 1D). Therefore, $GABA_{end}$ and GABA-d2 were detected in the same electropherogram but at different migration times (Fig. 1D). In this quantitative approach it is assumed that the conserved experimental setup and short time between injections minimizes variability compared to completely different runs [32]. We found that the results of endogenous GABA quantification were comparable with the on-line sampling approach (Table S8 and S10). Overall, this off-line sampling approach for quantitation was found to be simple, having lower risk of sample contamination and reasonable throughput. Therefore this method was chosen for further experiments.

The brain is a complex organ where cellular regions have distinct chemistry and chemical gradients that are essential to sustain life and function. The chemical distribution over the brain, or other organ, can be studied with MSI using various quantitative approaches to gain insights into the role of chemistry in function or dysfunction [33,34]. To investigate the applicability of the fifth approach for quantitative (Q) SS-CE-MS, four larger morphological regions, specifically cortex,

hippocampus, hypothalamus, and thalamus, of a regular brain tissue section were targeted for three samplings per region using 19 metabolite standards (Fig. 2, Table S9). The results show an overall similar concentration ranges of the individual metabolites in the four different brain regions (Fig. 2, Table S10 and S11). However, the method demonstrated quite high variation as determined by RSD (Table S11). This is attributed both to technical limitations during injection and to biological variations since the sampled regions sometimes were far apart, suggesting that different morphological regions were sampled (Fig. S4). The difference between regions becomes increasingly clear since the analytes vary independently between the sampled spots.

The obtained results revealed conserved ratios between important amino acids (Fig. S5), which is in agreement with the previous reports: quantitative studies of blood and cerebrospinal fluid (CSF) has indicated the significance of conserved relative amounts of alanine:lysine (3:1) and alanine:phenylalanine + tyrosine (4:1) in healthy systems [35]. Furthermore, our results show that the concentration of selected neurotransmitters are similar in all four brain areas but differ largely between the neurotransmitters (Fig. 2, Table S10 and S11). Specifically, acetylcholine was detected at minute amounts compared to GABA, glutamine, and glutamate (Fig. 2 and S6). It is well known that cellular homeostasis of glutamate is crucial and that the glutamate-glutamine cycle is one process for glutamate recycling through neurons and astrocytes [36]. Interestingly, the relative detected concentrations of glutamate:glutamine ratio show significant differences in the four regions, with the highest ratio being in the hippocampus and the lowest in the hypothalamus, indicating the role of glutamine in glutamate recycling varies in brain regions (Fig. S7). This suggests the applicability of Q–SS–CE-MS for studying cellular important processes in intact tissue.

Although most metabolites did not show statistically significant alterations across the brain regions in this proof-of-principle experiment, there are some exceptions. The most dynamic distributions were found in the aromatic amino acids tyrosine, phenylalanine, and tryptophan (Fig. 2 and S8, Table S10 and S11). Phenylalanine and tryptophan are essential amino acids that are actively transported over the blood brain barrier and serve as precursors for tyrosine and hydroxytryptophan, respectively, which in turn are precursors for dopamine and serotonin [37]. Despite tyrosine having the overall highest concentration, these three aromatic amino acids show similar concentration profiles in the regions with the highest abundances in the thalamus, which is in accordance with past research of the localization of tyrosine hydroxylase, tyrosine, and dopamine (Fig. 2 and S8) [38–40]. Overall, Q–SS–CE-MS can provide detailed information on the distribution of metabolites in cellular regions that is essential for further chemical mapping and understanding of brain function.

In addition to spatial mapping of metabolites, the step of separation with CE prior to MS enables differentiation and identification of isomers and isobars [13,16,28]. This includes the multiple species detected in the mass channels of alanine (*m/z* 90.0547), valine (*m/z* 118.0876), leucine (*m/z* 132.1011), and histidine (*m/z* 156.0758) (Fig. 3A). For example, three ions with different migration times are detected in the alanine mass channel, where the major peak correspond to alanine according to standard migration time. Additionally, the mass channel of leucine also includes isoleucine as confirmed by standards. Although base-line separation of leucine and isoleucine in CE is usually accomplished using a chiral modifier, such as β-cyclodextrin, their difference in electrophoretic mobility enables partial separation even with bare fused silica [41]. By Q–SS–CE-MS, we confirm that leucine is the most

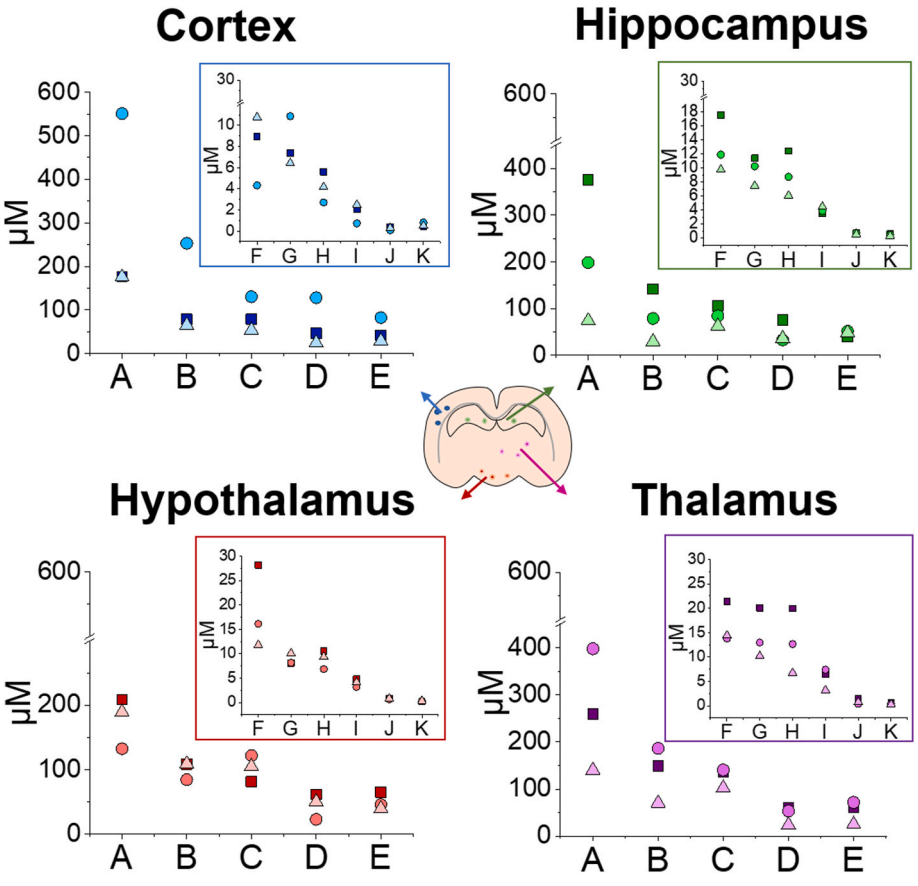

Fig. 2. Spatial metabolomics of 11 metabolites performed on four morphological regions in rat brain as depicted in the center schematic using Q–SS–CE-MS. All three samplings are plotted as squares, triangles and round dots. Plots with lower abundant metabolites are inserted in the plots with higher abundant analytes. List of metabolites: A – Glutamate, B – Glutamine, C – GABA, D – Serine, E – Alanine, F – Lysine, G – Arginine, H – Tyrosine, I – Phenylalanine, J – Tryptophan, K – Acetylcholine.

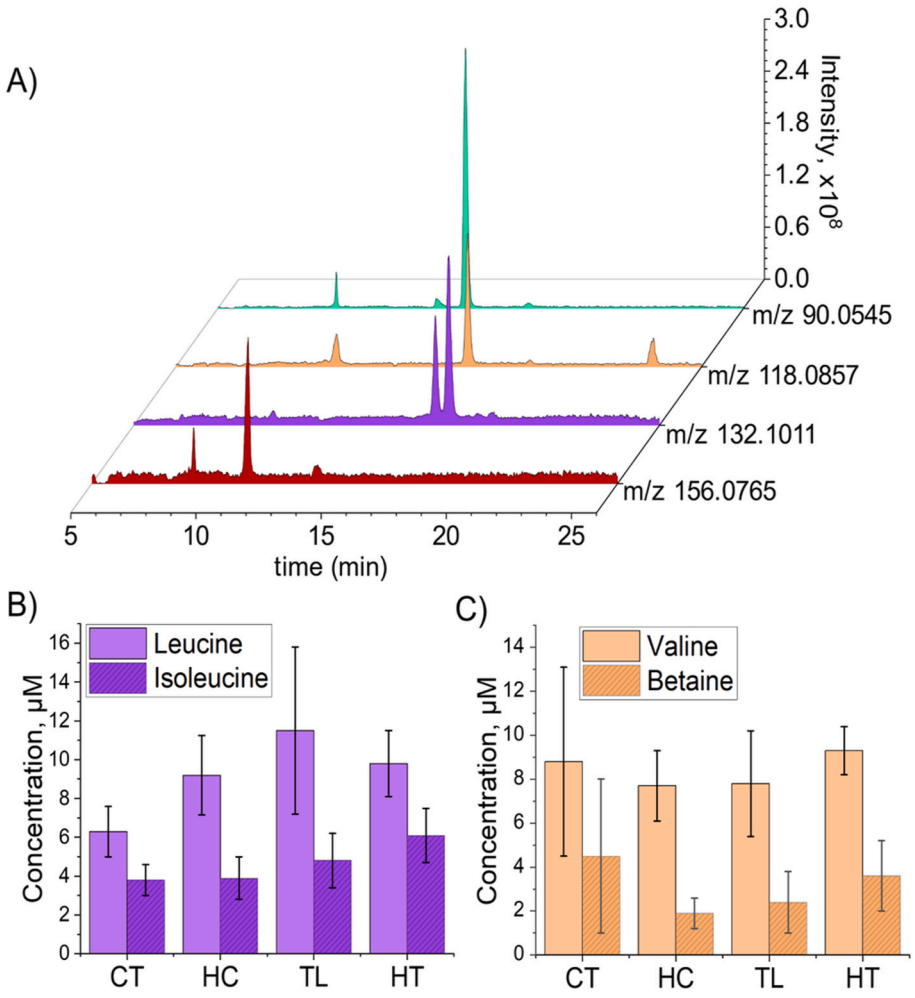

Fig. 3. Separation, identification and quantitation of isomeric species in rat brain tissue. a) four extracted ion electropherograms having multiple peaks: green - *m/z* 90.0545, orange - *m/z* 118.0857, purple - *m/z* 132.1011, and red - *m/z* 156.0765 (presented with 3 times increase in intensity); b) detected concentrations of leucine and isoleucine in four brain regions; c) detected concentrations of valine and betaine in four brain regions. CT – cortex, HC- hippocampus, TL-thalamus and HT – hypothalamus. Error bars represent one standard deviation from 3 sampling in each region. (For interpretation of the references to colour in this figure legend, the reader is referred to the Web version of this article.)

abundant isomers in all four brain regions. Furthermore, we find that the concentrations of the two isomers vary independently of each other with leucine being most abundant in the thalamus and isoleucine in the hypothalamus (Fig. 3B). Both leucine and isoleucine are essential amino acids that need to be absorbed from diet and passed through the blood-brain barrier [42]. In addition to protein synthesis, both isomers are believed to be important in signaling, although the role of isoleucine is less known than that of leucine, which includes activation of the mTOR signaling pathway [18]. Similarly, Q–SS–CE-MS enables spatial mapping of the isomer pair valine and betaine (*m/z* 118.0876) in all four brain regions. It is essential to characterize their spatial localization independently since their biological functions are diverse. While valine is a branched chain amino acid, similar to leucine and isoleucine, betaine is believed to serve as a neuroprotectant for neurodegenerative diseases [43]. Out of the two isomers, we find that valine is more abundant and that their profiles are similar in the four brain regions (Fig. 3C). With the assistance of Q–SS–CE-MS, we foresee designing experiments to map the importance of these isomers in biological function and processes.

4. Conclusions

In the present work, we described and evaluated approaches for quantification of metabolites in tissue using SS-CE-MS. We found that external calibration in BGE, brain extract, and mimetic tissue resulted in linear calibration curves, suggesting the applicability for quantitation with SS-CE-MS, but were more laborious than using one-point calibration. For one-point calibration strategies, we found that spiking a labelled internal standard into the extraction solvent contributed to contamination and that an off-line sequential injection of analyte followed by standard was the optimal solution. In addition to minimizing the analysis time by migrating both the analytes and the standards in the same run, the off-line sequential sampling approach does not require the purchase of labelled standards. The approach also showed validity when applied to sampling three individual locations in four morphological regions of rat brain, enabling us to report quantitative spatial metabolomics with isomeric specificity. Despite the biologically relevant results, it should be noted that the technique requires further refinement to reduce variability and improve precision. For example, the sampling area size can be decreased to account for the region heterogeneity and hydrodynamic injection can be investigated for reduced variability. Overall, we anticipate that this non-targeted approach for quantitative spatial metabolomics will be of great value in future studies deducing the chemical complexity connected to biological function.

CRediT authorship contribution statement

Anastasia Golubova: Writing – original draft, Visualization, Methodology, Investigation, Data curation, Conceptualization. **Ingela Lanekoff:** Writing – review & editing, Visualization, Validation, Supervision, Methodology, Funding acquisition, Conceptualization.

Declaration of competing interest

The authors declare that they have no known competing financial interests or personal relationships that could have appeared to influence the work reported in this paper.

Acknowledgements

Funding for this work was provided by the Swedish Foundation for Strategic Research (ITM17-0014).

Appendix A. Supplementary data

Supplementary data to this article can be found online at https://doi.org/10.1016/j.talanta.2025.128482.

Data availability

The data that support the findings of this study are available from the corresponding author upon reasonable request.

References

[1] A.R. Buchberger, K. DeLaney, J. Johnson, L. Li, Mass spectrometry imaging: a review of emerging advancements and future insights, Anal. Chem. 90 (2018) 240–265, https://doi.org/10.1021/acs.analchem.7b04733.
[2] J. Laskin, I. Lanekoff, Ambient mass spectrometry imaging using direct liquid extraction techniques, Anal. Chem. 88 (2016) 52–73, https://doi.org/10.1021/acs.analchem.5b04188.
[3] D. Unsihuay, P. Su, H. Hu, J. Qiu, S. Kuang, Y. Li, X. Sun, S.K. Dey, J. Laskin, Imaging and analysis of isomeric unsaturated lipids through online photochemical derivatization of carbon–carbon double bonds, Angew. Chem. Int. Ed. 60 (2021) 7559–7563, https://doi.org/10.1002/anie.202016734.
[4] J. Lillja, I. Lanekoff, Quantitative determination of sn-positional phospholipid isomers in MSn using silver cationization, Anal. Bioanal. Chem. 414 (2022) 7473–7482, https://doi.org/10.1007/s00216-022-04173-6.
[5] M.R.L. Paine, B.L.J. Poad, G.B. Eijkel, D.L. Marshall, S.J. Blanksby, R.M.A. Heeren, S.R. Ellis, Mass spectrometry imaging with isomeric resolution enabled by ozone-induced dissociation, Angew. Chem. Int. Ed. 57 (2018) 10530–10534, https://doi.org/10.1002/anie.201802937.
[6] T. Yan, Z. Liang, B.M. Prentice, Imaging and structural characterization of phosphatidylcholine isomers from rat brain tissue using sequential collision-induced Dissociation/electron-induced dissociation, Anal. Chem. 95 (2023) 15707–15715.
[7] J. Zhang, X. Huo, C. Guo, X. Ma, H. Huang, J. He, X. Wang, F. Tang, Rapid imaging of unsaturated lipids at an isomeric level achieved by controllable oxidation, Anal. Chem. 93 (2021) 2114–2124, https://doi.org/10.1021/acs.analchem.0c03888.
[8] E.S. Rivera, K.V. Djambazova, E.K. Neumann, R.M. Caprioli, J.M. Spraggins, Integrating ion mobility and imaging mass spectrometry for comprehensive analysis of biological tissues: a brief review and perspective, J. Mass Spectrom. 55 (2020) e4614, https://doi.org/10.1002/jms.4614.
[9] T. Alexandrov, J. Saez-Rodriguez, S.K. Saka, Enablers and challenges of spatial omics, a melting pot of technologies, Mol. Syst. Biol. 19 (2023) e10571, https://doi.org/10.15252/msb.202110571.
[10] Y. Zhu, P.D. Piehowski, R. Zhao, J. Chen, Y. Shen, R.J. Moore, A.K. Shukla, V. A. Petyuk, M. Campbell-Thompson, C.E. Mathews, R.D. Smith, W.-J. Qian, R. T. Kelly, Nanodroplet processing platform for deep and quantitative proteome profiling of 10–100 mammalian cells, Nat. Commun. 9 (2018) 882, https://doi.org/10.1038/s41467-018-03367-w.
[11] V. Kertesz, T.M. Weiskittel, G.J. Van Berkel, An enhanced droplet-based liquid microjunction surface sampling system coupled with HPLC-ESI-MS/MS for spatially resolved analysis, Anal. Bioanal. Chem. 407 (2015) 2117–2125, https://doi.org/10.1007/s00216-014-8287-5.
[12] B. Chen, M. Vavrek, M.T. Cancilla, V. Kertesz, Development and application of DropletProbe mass spectrometry for examining biodistribution of therapeutics, Methods Mol. Biol. (2022) 171–180.
[13] A. Golubova, I. Lanekoff, Surface sampling capillary electrophoresis–mass spectrometry for a direct chemical characterization of tissue and blood samples, Electrophoresis 44 (2023) 387–394, https://doi.org/10.1002/elps.202200183.
[14] V. Kertesz, T.M. Weiskittel, M. Vavrek, C. Freddo, G.J. Van Berkel, Extraction efficiency and implications for absolute quantitation of propranolol in mouse brain, liver and kidney tissue sections using droplet-based liquid microjunction surface sampling high-performance liquid chromatography/electrospray ionization tande: extraction efficiency and absolute quantitation of propranolol, Rapid Commun. Mass Spectrom. 30 (2016) 1705–1712, https://doi.org/10.1002/rcm.7607.
[15] V. Kertesz, M. Vavrek, C. Freddo, G.J. Van Berkel, Spatial profiling of stapled α–helical peptide ATSP-7041 in mouse whole-body thin tissue sections using droplet-based liquid microjunction surface sampling-HPLC-ESI–MS/MS, Int. J. Mass Spectrom. 437 (2019) 17–22, https://doi.org/10.1016/j.ijms.2018.01.005.
[16] K.D. Duncan, I. Lanekoff, Spatially defined surface sampling capillary electrophoresis mass spectrometry, Anal. Chem. 91 (2019) 7819–7827, https://doi.org/10.1021/acs.analchem.9b01516.
[17] H.-M. Lewis, R.P. Webb, G.F. Verbeck, J. Bunch, J. De Jesus, C. Costa, V. Palitsin, J. Swales, R.J.A. Goodwin, P. Sears, M.J. Bailey, Nanoextraction coupled to liquid chromatography mass spectrometry delivers improved spatially resolved analysis, Anal. Chem. 91 (2019) 15411–15417, https://doi.org/10.1021/acs.analchem.9b02821.
[18] S. Zhang, X. Zeng, M. Ren, X. Mao, S. Qiao, Novel metabolic and physiological functions of branched chain amino acids: a review, J. Anim. Sci. Biotechnol. 8 (2017) 10, https://doi.org/10.1186/s40104-016-0139-z.
[19] A.J. Taylor, A. Dexter, J. Bunch, Exploring ion suppression in mass spectrometry imaging of a heterogeneous tissue, Anal. Chem. 90 (2018) 5637–5645, https://doi.org/10.1021/acs.analchem.7b05005.
[20] I. Lanekoff, S.L. Stevens, M.P. Stenzel-Poore, J. Laskin, Matrix effects in biological mass spectrometry imaging: identification and compensation, Analyst 139 (2014) 3528, https://doi.org/10.1039/c4an00504j.
[21] C.W. Chumbley, M.L. Reyzer, J.L. Allen, G.A. Marriner, L.E. Via, C.E. Barry, R. M. Caprioli, Absolute quantitative MALDI imaging mass spectrometry: a case of rifampicin in liver tissues, Anal. Chem. 88 (2016) 2392–2398, https://doi.org/10.1021/acs.analchem.5b04409.
[22] I. Lanekoff, J. Laskin, Quantitative mass spectrometry imaging of molecules in biological systems. Advances in Chromatography, 2017.
[23] Daisy Unsihuay, Daniela Mesa Sanchez, Julia Laskin, Quantitative mass spectrometry imaging of biological systems, Annu. Rev. Phys. Chem. 72 (2021), https://doi.org/10.1146/annurev-physchem-061020-053416.
[24] J. Barry, J.A. Barry, M.R. Groseclose, D.D. Fraser, S. Castellino, Revised Preparation of a Mimetic Tissue Model for Quantitative Imaging Mass Spectrometry, Protocol Exchange, 2018, https://doi.org/10.1038/protex.2018.104.
[25] D. Eikel, M. Vavrek, S. Smith, C. Bason, S. Yeh, W.A. Korfmacher, J.D. Henion, Liquid extraction surface analysis mass spectrometry (LESA-MS) as a novel profiling tool for drug distribution and metabolism analysis: the terfenadine example, Rapid Commun. Mass Spectrom. 25 (2011) 3587–3596, https://doi.org/10.1002/rcm.5274.
[26] D. Veličković, R.K. Chu, A.A. Carrell, M. Thomas, L. Paša-Tolić, D.J. Weston, C. R. Anderton, Multimodal MSI in conjunction with broad coverage spatially resolved MS^2 increases confidence in both molecular identification and localization, Anal. Chem. 90 (2018) 702–707, https://doi.org/10.1021/acs.analchem.7b04319.
[27] Q. Wu, Z. Huang, Y. Wang, Z. Zhang, H. Lu, Absolute quantitative imaging of sphingolipids in brain tissue by exhaustive liquid microjunction surface sampling–liquid chromatography–mass spectrometry, J. Chromatogr. A 1609 (2020) 460436, https://doi.org/10.1016/j.chroma.2019.460436.
[28] Q. Wu, Y. Li, Y. Wang, H. Lu, Quantitative mass spectrometry imaging of amino acids with isomer differentiation in brain tissue via exhaustive liquid microjunction surface sampling–tandem mass tags labeling–ultra performance liquid chromatography–mass spectrometry, J. Chromatogr. A 1621 (2020) 461086, https://doi.org/10.1016/j.chroma.2020.461086.
[29] M.C. Breadmore, Electrokinetic and hydrodynamic injection: making the right choice for capillary electrophoresis, Bioanalysis 1 (2009) 889–894, https://doi.org/10.4155/bio.09.73.
[30] A. Traberg, F.E. Pinto, A.C.N. Hansen, M. Haedersdal, C.M. Lerche, C. Janfelt, Quantitative mass spectrometry imaging of bleomycin in skin using a mimetic tissue model for calibration, Pharmaceuticals 15 (2022) 1583, https://doi.org/10.3390/ph15121583.
[31] N.L. Kuehnbaum, A. Kormendi, P. Britz-McKibbin, Multisegment injection-capillary electrophoresis-mass spectrometry: a high-throughput platform for metabolomics with high data fidelity, Anal. Chem. 85 (2013) 10664–10669, https://doi.org/10.1021/ac403171u.
[32] I. Lanekoff, M. Thomas, J. Laskin, Shotgun approach for quantitative imaging of phospholipids using nanospray desorption electrospray ionization mass spectrometry, Anal. Chem. 86 (2014) 1872–1880, https://doi.org/10.1021/ac403931r.
[33] M. Vandenbosch, S.M. Mutuku, M.J.Q. Mantas, N.H. Patterson, T. Hallmark, M. Claesen, R.M.A. Heeren, N.G. Hatcher, N. Verbeeck, K. Ekroos, S.R. Ellis, Toward omics-scale quantitative mass spectrometry imaging of lipids in brain tissue using a multiclass internal standard mixture, Anal. Chem. 95 (2023) 18719–18730, https://doi.org/10.1021/acs.analchem.3c02724.
[34] R.R. Kibbe, D.C. Muddiman, Quantitative mass spectrometry imaging (qMSI): a tutorial, J. Mass Spectrom. 59 (2024) e5009, https://doi.org/10.1002/jms.5009.
[35] R.H. Haas, S. Parikh, M.J. Falk, R.P. Saneto, N.I. Wolf, N. Darin, L.-J. Wong, B. H. Cohen, R.K. Naviaux, The in-depth evaluation of suspected mitochondrial disease, Mol. Genet. Metabol. 94 (2008) 16–37, https://doi.org/10.1016/j.ymgme.2007.11.018.

[36] J.V. Andersen, K.H. Markussen, E. Jakobsen, A. Schousboe, H.S. Waagepetersen, P. A. Rosenberg, B.I. Aldana, Glutamate metabolism and recycling at the excitatory synapse in health and neurodegeneration, Neuropharmacology 196 (2021) 108719, https://doi.org/10.1016/j.neuropharm.2021.108719.
[37] E. Höglund, Ø. Øverli, S. Winberg, Tryptophan metabolic pathways and brain serotonergic activity: a comparative review, Front. Endocrinol. 10 (2019) 158, https://doi.org/10.3389/fendo.2019.00158.
[38] M.G. Bilbao, D. Garrigos, M. Martinez-Morga, A. Toval, Y. Kutsenko, R. Bautista, A. Barreda, B. Ribeiro Do-Couto, L. Puelles, J.L. Ferran, Prosomeric hypothalamic distribution of tyrosine hydroxylase positive cells in adolescent rats, Front. Neuroanat. 16 (2022) 868345, https://doi.org/10.3389/fnana.2022.868345.
[39] M. Shariatgorji, A. Nilsson, R.J.A. Goodwin, P. Källback, N. Schintu, X. Zhang, A. R. Crossman, E. Bezard, P. Svenningsson, P.E. Andren, Direct targeted quantitative molecular imaging of neurotransmitters in brain tissue sections, Neuron 84 (2014) 697–707, https://doi.org/10.1016/j.neuron.2014.10.011.
[40] M.Á. Sánchez-González, M.Á. García-Cabezas, B. Rico, C. Cavada, The primate thalamus is a key target for brain dopamine, J. Neurosci. 25 (2005) 6076–6083, https://doi.org/10.1523/JNEUROSCI.0968-05.2005.
[41] C. Boniglia, B. Carratù, E. Sanzini, Enantiomer separation of D-L branched amino acids by capillary electrophoresis in sport nutritional supplements, J. Food Sci. 67 (2002) 1352–1355, https://doi.org/10.1111/j.1365-2621.2002.tb10287.x.
[42] J.D. Fernstrom, Branched-chain amino acids and brain function, J. Nutr. 135 (2005) 1539S–1546S, https://doi.org/10.1093/jn/135.6.1539S.
[43] M. Bhatt, A. Di Iacovo, T. Romanazzi, C. Roseti, E. Bossi, Betaine—the dark knight of the brain, Basic Clin. Pharmacol. Toxicol. 133 (2023) 485–495, https://doi.org/10.1111/bcpt.13839.